esteem3

Enabling Science through European Electron Microscopy

Report on correlation spectral imaging

Deliverable D5.4– version 1.1

Estimated delivery date:	April 30th 2023
Actual delivery date:	March 23rd 2023
Lead beneficiary:	CNRS LPS
Person responsible:	Luiz Tizei
Deliverable type:	☒ R ☐ DEM ☐ DEC ☐ OTHER ☐ ETHICS ☐ ORDP
Dissemination level:	PUBLIC

Grant Agreement No:	823717
Funding Instrument:	Research and Innovation Actions (RIA)
Funded under:	H2020-INFRAIA-2018-1: Integrating Activities for Advanced Communities
Starting date:	01.01.2019
Duration:	54 months

THIS PROJECT HAS RECEIVED FUNDING FROM THE EUROPEAN UNION'S HORIZON 2020 RESEARCH AND INNOVATION PROGRAMME UNDER GRANT AGREEMENT NO **823717**

Revision history log

Version number	Date of release	Author	Summary of changes
V0.1	22/03/2023	Luiz Tizei	First draft of the deliverable
V1	22/03/2023	Peter A. van Aken	Minor amendments and approval
V1.1	22/03/2023	Aude Garsès	General review and minor amendments

Cathodoluminescence excitation spectroscopy: Nanoscale imaging of excitation pathways

We report on time correlation experiments between energy absorption from an electron and photon emission from a sample. The correlated electron-photon events give rise to a spectrum, which we call cathodoluminescence excitation (CLE) spectrum. It is different from an electron energy loss spectrum (EELS), as only those electrons leading to light emission, or cathodoluminescence (CL), are counted. The ratio of CLE to EELS spectra is a measurement of the material relative quantum efficiency for light emission, which can be mapped with nanometer spatial resolution.[1]

Coincidences and relative quantum efficiency measurement

Electron scattering in matter leads to light emission through different processes, extending in wide energy (from millielectron to kilo–electron volt) and time (from femtosecond to microsecond) ranges. In Figure 1, optical transitions are represented by vertical arrows and relaxation pathways by black arrows, with qualitative temporal axis from left to right. To understand CLE, it is necessary to know how EELS and CL spectra relate to the processes described in Figure 1. Every inelastically scattered electron must undergo a first excitation (purple arrow in Figure 1) that can be measured with EELS. This encompasses transition radiation (TR), near-band-edge (NBE) excitations, core-level excitations[2], bulk[3] and surface[4] plasmon excitations, phonon excitations[5,6], and exciton excitations[7]. TR occurs when a relativistic electron crosses a dielectric discontinuity and is often missed in the presence of other excitations in the same energy range, because of its small oscillator strength. The NBE of semiconductors is easily detected in EELS, especially with modern electron monochromator technologies[6]. Core-electron spectroscopy is widely used for chemical mapping and allotrope identification[2] down to the atomic scale[8].

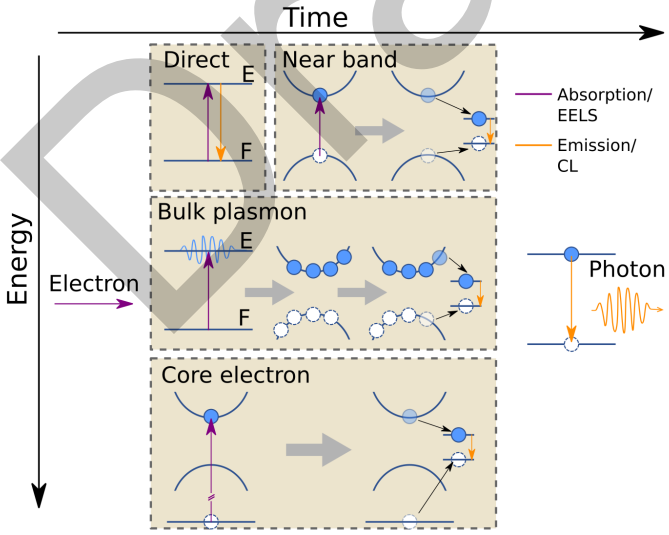

Figure 1: **Excitation and decay pathways.** Different excitations can be created in materials under electron (purple) irradiation. These excitations can eventually decay into photons (orange). As these events are linked in time, electron-photon time coincidences tell us, which energies are more efficient for photon generation.

After having been created through the above-detailed absorption process revealed by EELS, these distinct excitations over a wide range of energies can lead to photon emission, detected with CL in the infrared-ultraviolet range, through different relaxation pathways, some of which are still not understood. TR and SP are typical of photonic materials, characterized by a phase-locked emitted photon relative to the exciting electrons[9]. Therefore, extinction (EELS) and emission (CL) spectra are similar, with only slight shifts expected[10], and therefore, we expect a CLE spectrum to closely resemble a CL spectrum. In luminescent materials, absorption and decay pathways are expected to be more complex upon electron

excitation. As depicted in Figure 1, NBE, bulk plasmons, core-level excitations, or direct excitations can lead to the emission of light, and we expect the CLE to be quite different from the EELS. A microscopic description of the weight of each of the energy transfer processes is still not available.

An emission (CL) event is necessarily preceded by an absorption or extinction event at a given energy (EELS). This relation is temporal in nature and lost in commonly time-averaged EELS spectra, where all potential EELS events corresponding to the same emission are summed. It is, however, stored in the probability of each electron scattering event and photon emission. This can be retrieved by generating coincidence histograms of electron energy-loss and photon emission events (described in what follows; in Figure 2A and B). Coincidence electron spectroscopy and microscopy have been performed in the past, for example, coincidence of EELS with secondary electron or x-ray emission[11–13]. EELS-CL coincidence has been performed for discrete selected EELS energy ranges[14,15], but the relative QE as a function of energy and its spatial dependence has not been measured. To achieve CLE, a temporal resolution below the time interval between events, given by the electron current (typically 1 electron every 16 ns for 10 pA), is needed for all energy-loss events of interest.

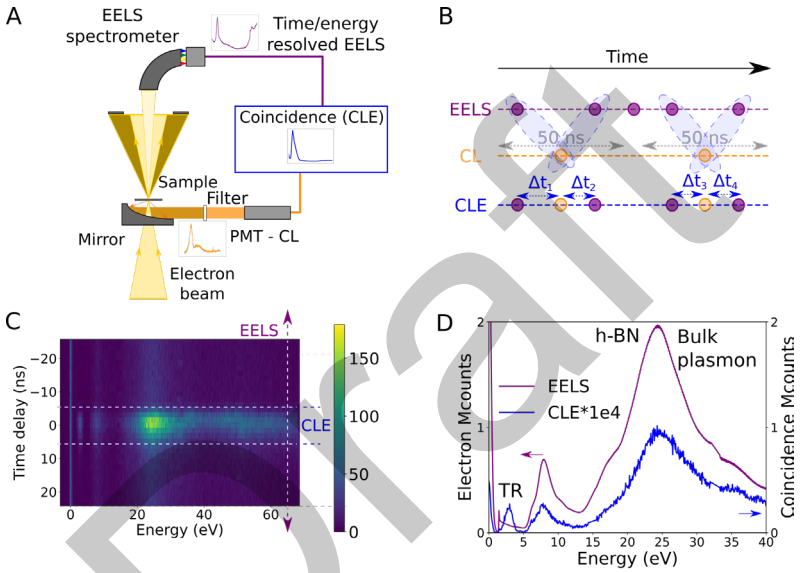

Figure 2: ***Experimental setup and CLE.*** *(A) The CLE experiment was setup in a STEM equipped with a light injector/collector for photons (CL) detection (orange) and an EELS spectrometer (purple). Electrons and photons were detected using nanosecond-resolved detectors. (B) Electron-photon coincident pairs were sought in list of events using a search algorithm. (C) From these, time-delay and energy 2D histograms are constructed. (C-D) An EELS spectrum is measured by integrating all electrons detected, while the CLE spectrum only contains those separated by a short time from a photon.*

With this in mind, we implemented an EELS-CL setup in a STEM, displayed in Figure 2A. In Figure 2, we illustrate the principle of CLE on the simplest case of the plasmonic particles. For EELS, a Timepix3 detector was used[16]. The detector supplies sub–10-ns time resolution over arbitrary energy ranges decided by the resolution power of the electron spectrometer and the Timepix3 pixel size. In addition, the detector used (CheeTah, from Amsterdam Scientific Instruments) has two time-to-digital converters (TDCs), allowing to append timestamps from external signals into the original electron data flow. Photon emission events were detected with a photomultiplier tube (PMT) working in the 2.0- to 5.0-eV energy range. The PMT output is directly connected to one of the Timepix3 TDC lines. Electron and photon arrival times were stored in a list, along with the electron energy loss. The response time of the detection scheme is ≈5 to 25 ns. We used a search algorithm (the code available at Zenodo[17]) to find electrons that are within ±25 ns of a detected photon, from which a 2D histogram of time delay versus

electron energy loss is reconstructed (Figure 2C). This 2D histogram shows the temporal evolution of the loss spectrum as a function of delay to a detected photon.

From these, we reconstructed a 2D histogram of electron energy-loss events as a function of time delay to a photon emission (Figure 2C). Because of the typical lifetimes of the CL events (SP and TR in sub-picoseconds and defect emission in sub-nanoseconds), the CLE spectrum is extracted from the shortest time delays given the time response of the experiment (±5 ns), within which coincidence above the long delay limit was seen. For longer lifetimes, larger time integration should be considered. The CLE spectrum resembles an EELS spectrum but weighted by the photon emission probability (Figure 2D). Last, the ratio of the CLE and the non-coincidence EELS therefore provides the relative QE of different absorption processes (Figure 3). It highlights differences between competitive radiative and nonradiative pathways.

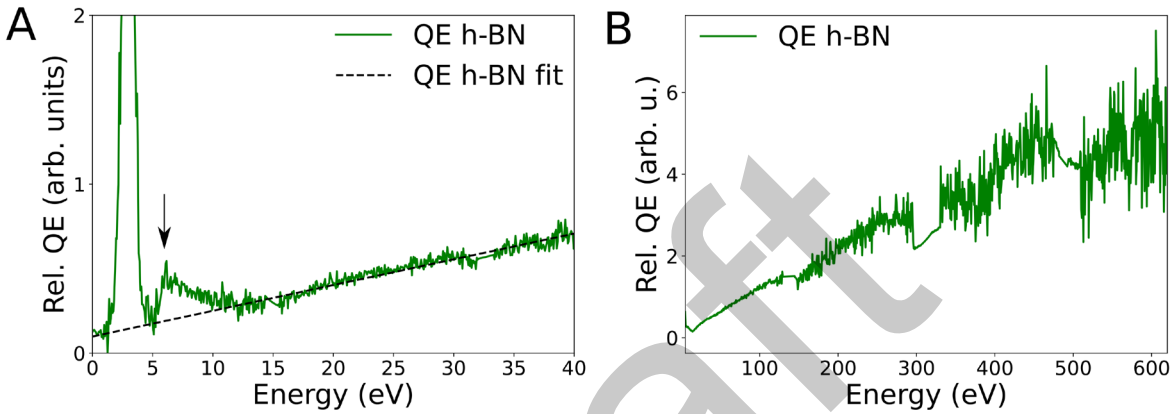

Figure 3: **Relative quantum efficience.** (A-B) The relative quantum efficiency (QE) is given by the ratio of the CLE and EELS spectra. Energy losses close to the NBE of h-BN (~6 eV) are efficient towards light emission. The current signal-to-noise ratio prevents the observation of fine structures for core-losses (B).

Now that the principle of the CLE is established, we turn to the possibility of mapping the different pathways directly in real space. The proposed spectroscopy scheme allows for coincidence mapping, of which more details are reported elsewhere (*35*). The 4.1-eV emission in *h*-BN is known to arise from single point defects (*24*). For each single defect, the CL excitation area forms an intensity spot of ≈80 × 80 nm^2 wide. We performed CLE mapping by rastering a nanometer-sized beam on the sample and collecting a full CLE spectrum corresponding to emission in the 3.65- to 4.13-eV range at each pixel of the scan. From this, CLE maps can be created by filtering over different absorption (EELS) ranges.

These time-resolved maps permit disentangling the different decay pathways in space and energy, with a 32-nm spatial sampling. The two bright features in the image are separated by 125 nm. The CLE map filtered above 6.5-eV energy loss shows two sharply localized intensity spots consistent with the observation of 4.1-eV localized defects (Figure 4A). On the contrary, the CLE map filtered between 2 and 5 eV (Figure 4B), on the peak linked to TR, shows that both the *h*-BN flake and the thin amorphous carbon support exhibit coincidence events distributed in a relatively uniform manner. We note that we could not identify any specific absorption signature of the defects at their absorption energy. Coincidence measurements with better EELS spectral resolution might reveal it in the future.

Also, the spatial resolution is essentially dependent on that of the CL, which is limited by the diffusion lengths in the materials. One can expect a few nanometers of spatial resolution in other materials, such as III-N heterostructures[18].

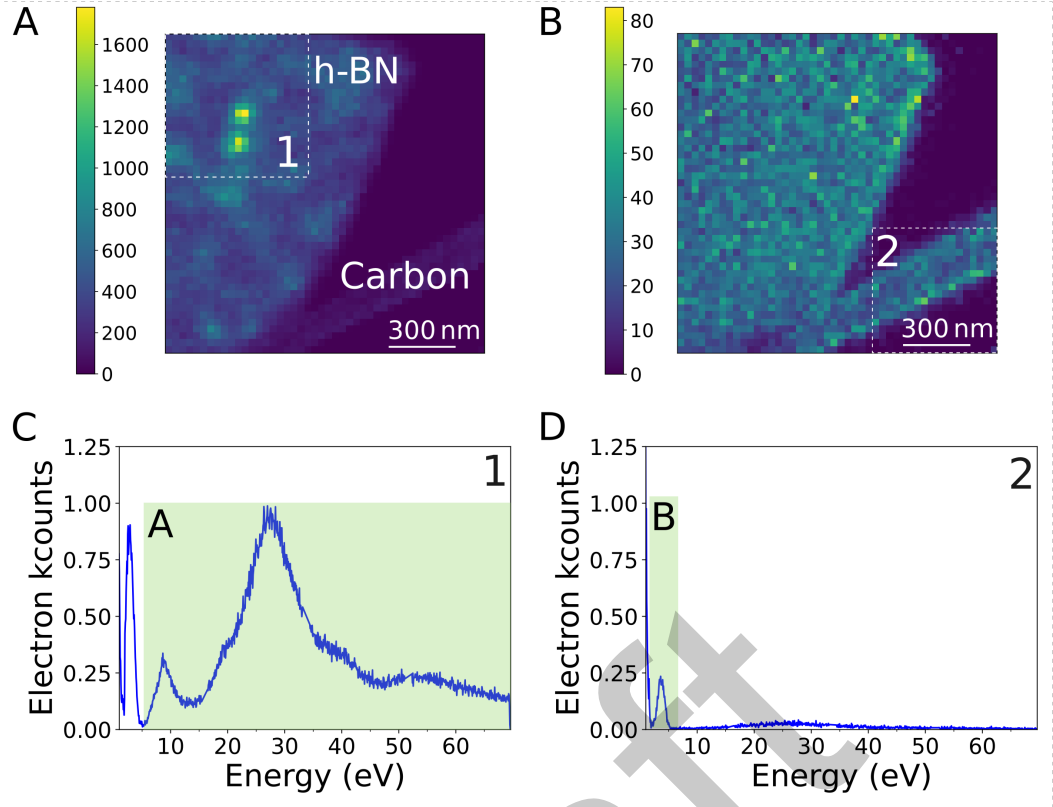

Figure 4: **Spatially resolved CLE maps in *h*-BN.** (A) CLE energy-filtered map above 6.5 eV, the NBE energy, showing multiple localized absorption maxima that lead to the emission of the 4.1-eV defect. (B) CLE energy-filtered map between 2 and 5 eV, showing where TR occurs. Both the *h*-BN thin flake and the amorphous carbon support (bottom right, which is the support for *h*-BN in the TEM sample) show absorption leading to photon emission. (C and D) CLE spectra of regions marked 1 and 2 in (A) and (B), with marked integrated ranges for maps A and B, respectively

Methods

Coincidence EELS-CL experiments were performed on a modified Vacuum Generator (VG) HB501 STEM (Scanning Transmission Electron Microscope) equipped with a cold field-emission source, an Attolight Mönch light collection system, a liquid nitrogen–cooled sample stage, and a Cheetah Timepix3 (manufactured by Amsterdam Scientific Instruments) event-based direct electron detector. More details about the experimental setup and event-based detection can be found in the work of Auad et al.[16]. The beam current in coincidence measurements was typically from 1 to 10 pA, and a convergence half-angle of 7.5 mrad was used.

Conclusion and Perspective

In conclusion, we showed spatially resolved CLE, which encompasses the main advantages of photoluminescence excitation (PLE) spectroscopy (high-sensitivity measurement of the relative QE and consequent insight between multiple light emission decay pathways) with that of electron spectroscopies (wide energy range and nanometer-scale spatial resolution). Numerous applications of CLE are expected for nanomaterials, ranging from the optimization of single-photon sources[19], the unveiling of the role of nanometer- to atomic-scale features on the optical properties of transition metal dichalcogenide monolayers by mapping the excitons' binding energy[20,21], to the characterization of previously unknown optical materials such as hybrid perovskites[22] and others yet to be found and understood. The spectromicroscopy scheme described requires only time-resolved electron and photon detectors, being implementable in any electron microscope. Therefore, it applies to any object compatible with STEM observation, should they be photonic (plasmonics systems, photonic bandgap materials and waveguides)

or luminescent (quantum wells, quantum dots, and single-photon emitters)[18,23]. The current applications of the setup in the time domain are limited by the electron detector temporal resolution. Improvements are expected with the new Timepix4 detector[24] soon, with fast deflectors or with the use of pulsed electron guns[25–27]. Photon and electron energy-resolved experiments in the core-level range with better temporal resolution should give further hints on the microscopic physics behind the relaxation pathways. In addition, as the number of emitted photons per electron per energy is lost using single-pixel detectors, the use of multiple PMTs or 2D arrays of detectors solves this, giving access to excitation energy–resolved Hanbury Brown and Twiss interferometry[28] for energy-resolved retrieval of quantum statistics, energy efficiency for total photon yield, and excited energy-resolved bunching experiments[29]. As for PLE, this technique resolved in emission and absorption energy will allow one to assign specific energy bands to each observed transition but now with nanoscale spatial resolution. Last, polarization-dependent EELS[30,31] and CL will give us an almost ideal nano-optics to probe excitation symmetries.

References:

(1) Varkentina, N.; Auad, Y.; Woo, S. Y.; Zobelli, A.; Bocher, L.; Blazit, J.-D.; Li, X.; Tencé, M.; Watanabe, K.; Taniguchi, T.; Stéphan, O.; Kociak, M.; Tizei, L. H. G. Cathodoluminescence Excitation Spectroscopy: Nanoscale Imaging of Excitation Pathways. *Sci. Adv.* **2022**, *8* (40), eabq4947. https://doi.org/10.1126/sciadv.abq4947.

(2) Egerton, R. F.; Egerton, R. *Electron Energy-Loss Spectroscopy in the Electron Microscope*, 3. ed.; Springer: New York Heidelberg, 2011.

(3) Raether, H. *Excitation of Plasmons and Interband Transitions by Electrons*; Springer Berlin: Berlin, 2013.

(4) Batson, P. E. A New Surface Plasmon Resonance in Clusters of Small Aluminum Spheres. *Ultramicroscopy* **1982**, *9* (3), 277–282. https://doi.org/10.1016/0304-3991(82)90212-1.

(5) Ibach, H. *Electron Energy Loss Spectroscopy and Surface Vibrations - 1st Edition*; Elsevier, 1982.

(6) Krivanek, O. L.; Lovejoy, T. C.; Dellby, N.; Aoki, T.; Carpenter, R. W.; Rez, P.; Soignard, E.; Zhu, J.; Batson, P. E.; Lagos, M. J.; Egerton, R. F.; Crozier, P. A. Vibrational Spectroscopy in the Electron Microscope. *Nature* **2014**, *514* (7521), 209–212. https://doi.org/10.1038/nature13870.

(7) Bonnet, N.; Lee, H. Y.; Shao, F.; Woo, S. Y.; Blazit, J.-D.; Watanabe, K.; Taniguchi, T.; Zobelli, A.; Stéphan, O.; Kociak, M.; Gradečak, S.; Tizei, L. H. G. Nanoscale Modification of WS_2 Trion Emission by Its Local Electromagnetic Environment. *Nano Lett.* **2021**, *21* (24), 10178–10185. https://doi.org/10.1021/acs.nanolett.1c02600.

(8) Muller, D. A.; Kourkoutis, L. F.; Murfitt, M.; Song, J. H.; Hwang, H. Y.; Silcox, J.; Dellby, N.; Krivanek, O. L. Atomic-Scale Chemical Imaging of Composition and Bonding by Aberration-Corrected Microscopy. *Science* **2008**, *319* (5866), 1073–1076. https://doi.org/10.1126/science.1148820.

(9) García de Abajo, F. J. Optical Excitations in Electron Microscopy. *Rev. Mod. Phys.* **2010**, *82* (1), 209–275. https://doi.org/10.1103/RevModPhys.82.209.

(10) Losquin, A.; Zagonel, L. F.; Myroshnychenko, V.; Rodríguez-González, B.; Tencé, M.; Scarabelli, L.; Förstner, J.; Liz-Marzán, L. M.; García de Abajo, F. J.; Stéphan, O.; Kociak, M. Unveiling Nanometer Scale Extinction and Scattering Phenomena through Combined Electron Energy Loss Spectroscopy and Cathodoluminescence Measurements. *Nano Lett.* **2015**, *15* (2), 1229–1237. https://doi.org/10.1021/nl5043775.

(11) Jannis, D.; Müller-Caspary, K.; Béché, A.; Oelsner, A.; Verbeeck, J. Spectroscopic Coincidence Experiments in Transmission Electron Microscopy. *Appl. Phys. Lett.* **2019**, *114* (14), 143101. https://doi.org/10.1063/1.5092945.

(12) Jannis, D.; Müller-Caspary, K.; Béché, A.; Verbeeck, J. Coincidence Detection of EELS and EDX Spectral Events in the Electron Microscope. *Appl. Sci.* **2021**, *11* (19), 9058. https://doi.org/10.3390/app11199058.

(13) Kruit, P.; Shuman, H.; Somlyo, A. P. Detection of X-Rays and Electron Energy Loss Events in Time Coincidence. *Ultramicroscopy* **1984**, *13* (3), 205–213. https://doi.org/10.1016/0304-3991(84)90199-2.

(14) Ahn, C. C.; Krivanek, O. L. Excited State Lifetime Measurements by EELS-CL Coincidence. In *Proc. 43rd Annual Meet. of the Electron Microscopy Soc. Am.*; 1985; pp 406–407.

(15) Graham, R. J.; Spence, J. C. H.; Alexander, H. Infrared Cathodoluminescence Studies from Dislocations in Silicon in Tem, a Fourier Transform Spectrometer for Cl in Tem and Els/Cl Coincidence Measurements of Lifetimes in Semiconductors. *MRS Online Proc. Libr.* **1986**, *82* (1), 235–245. https://doi.org/10.1557/PROC-82-235.
(16) Auad, Y.; Walls, M.; Blazit, J.-D.; Stéphan, O.; Tizei, L. H. G.; Kociak, M.; De la Peña, F.; Tencé, M. Event-Based Hyperspectral EELS: Towards Nanosecond Temporal Resolution. *Ultramicroscopy* **2022**, *239*, 113539. https://doi.org/10.1016/j.ultramic.2022.113539.
(17) Auad, Yves; Kociak, Mathieu; Tizei, Luiz H. G.; Blazit, Jean-Denis; Walls, Michael; Stéphan, Odile; De la Peña, Francisco; Tencé, Marcel. TimeSTEM/Tp3_tools: Release v1.0.0, 2022. https://doi.org/10.5281/ZENODO.6346261.
(18) Kociak, M.; Zagonel, L. F. Cathodoluminescence in the Scanning Transmission Electron Microscope. *Ultramicroscopy* **2017**, *176*, 112–131. https://doi.org/10.1016/j.ultramic.2016.11.018.
(19) Beha, K.; Batalov, A.; Manson, N. B.; Bratschitsch, R.; Leitenstorfer, A. Optimum Photoluminescence Excitation and Recharging Cycle of Single Nitrogen-Vacancy Centers in Ultrapure Diamond. *Phys. Rev. Lett.* **2012**, *109* (9), 097404. https://doi.org/10.1103/PhysRevLett.109.097404.
(20) Hill, H. M.; Rigosi, A. F.; Roquelet, C.; Chernikov, A.; Berkelbach, T. C.; Reichman, D. R.; Hybertsen, M. S.; Brus, L. E.; Heinz, T. F. Observation of Excitonic Rydberg States in Monolayer MoS2 and WS2 by Photoluminescence Excitation Spectroscopy. *Nano Lett.* **2015**, *15* (5), 2992–2997. https://doi.org/10.1021/nl504868p.
(21) Robert, C.; Semina, M. A.; Cadiz, F.; Manca, M.; Courtade, E.; Taniguchi, T.; Watanabe, K.; Cai, H.; Tongay, S.; Lassagne, B.; Renucci, P.; Amand, T.; Marie, X.; Glazov, M. M.; Urbaszek, B. Optical Spectroscopy of Excited Exciton States in ${\mathrm{MoS}}_{2}$ Monolayers in van Der Waals Heterostructures. *Phys. Rev. Mater.* **2018**, *2* (1), 011001. https://doi.org/10.1103/PhysRevMaterials.2.011001.
(22) Zelewski, S. J.; Urban, J. M.; Surrente, A.; Maude, D. K.; Kuc, A.; Schade, L.; Johnson, R. D.; Dollmann, M.; Nayak, P. K.; Snaith, H. J.; Radaelli, P.; Kudrawiec, R.; Nicholas, R. J.; Plochocka, P.; Baranowski, M. Revealing the Nature of Photoluminescence Emission in the Metal-Halide Double Perovskite Cs2AgBiBr6. *J. Mater. Chem. C* **2019**, *7* (27), 8350–8356. https://doi.org/10.1039/C9TC02402F.
(23) Polman, A.; Kociak, M.; García de Abajo, F. J. Electron-Beam Spectroscopy for Nanophotonics. *Nat. Mater.* **2019**. https://doi.org/10.1038/s41563-019-0409-1.
(24) Campbell, M.; Alozy, J.; Ballabriga, R.; Frojdh, E.; Heijne, E.; Llopart, X.; Poikela, T.; Tlustos, L.; Valerio, P.; Wong, W. Towards a New Generation of Pixel Detector Readout Chips. *J. Instrum.* **2016**, *11* (01), C01007. https://doi.org/10.1088/1748-0221/11/01/C01007.
(25) Barwick, B.; Flannigan, D. J.; Zewail, A. H. Photon-Induced near-Field Electron Microscopy. *Nature* **2009**, *462* (7275), 902–906. https://doi.org/10.1038/nature08662.
(26) Feist, A.; Echternkamp, K. E.; Schauss, J.; Yalunin, S. V.; Schäfer, S.; Ropers, C. Quantum Coherent Optical Phase Modulation in an Ultrafast Transmission Electron Microscope. *Nature* **2015**, *521* (7551), 200–203. https://doi.org/10.1038/nature14463.
(27) Houdellier, F.; Caruso, G. M.; Weber, S.; Kociak, M.; Arbouet, A. Development of a High Brightness Ultrafast Transmission Electron Microscope Based on a Laser-Driven Cold Field Emission Source. *Ultramicroscopy* **2018**, *186*, 128–138. https://doi.org/10.1016/j.ultramic.2017.12.015.
(28) Tizei, L. H. G.; Kociak, M. Spatially Resolved Quantum Nano-Optics of Single Photons Using an Electron Microscope. *Phys. Rev. Lett.* **2013**, *110*. https://doi.org/10.1103/PhysRevLett.110.153604.
(29) Meuret, S.; Tizei, L. H. G.; Cazimajou, T.; Bourrellier, R.; Chang, H. C.; Treussart, F.; Kociak, M. Photon Bunching in Cathodoluminescence. *Phys. Rev. Lett.* **2015**, *114*. https://doi.org/10.1103/PhysRevLett.114.197401.
(30) Guzzinati, G.; Béché, A.; Lourenço-Martins, H.; Martin, J.; Kociak, M.; Verbeeck, J. Probing the Symmetry of the Potential of Localized Surface Plasmon Resonances with Phase-Shaped Electron Beams. *Nat. Commun.* **2017**, 14999. https://doi.org/10.1038/ncomms14999.

(31) Lourenço-Martins, H.; Gérard, D.; Kociak, M. Optical Polarization Analogue in Free Electron Beams. *Nat. Phys.* **2021**. https://doi.org/10.1038/s41567-021-01163-w.